BIOCHEMISTRY
including biophysical chemistry & molecular biology

Article

pubs.acs.org/biochemistry

Identification of Amino Acids at the Catalytic Site of a Ferredoxin-Dependent Cyanobacterial Nitrate Reductase

Anurag P. Srivastava,[†] James P. Allen,[‡] Brian J. Vaccaro,[§] Masakazu Hirasawa,[†] Suzanne Alkul,[†,⊥] Michael K. Johnson,[§] and David B. Knaff*[,†,∥]

[†]Department of Chemistry and Biochemistry, Texas Tech University, Lubbock, Texas 79409-1061, United States
[‡]Department of Chemistry and Biochemistry, Arizona State University, Tempe, Arizona 85287-1604, United States
[§]Department of Chemistry and Center for Metalloenzyme Studies, University of Georgia, Athens, Georgia 30602-2556, United States
[∥]Center for Biotechnology and Genomics, Texas Tech University, Lubbock, Texas 79409-3132, United States

ABSTRACT: An *in silico* model of the ferredoxin-dependent nitrate reductase from the cyanobacterium *Synechococcus* sp. PCC 7942, and information about active sites in related enzymes, had identified Cys148, Met149, Met306, Asp163, and Arg351 as amino acids likely to be involved in either nitrate binding, prosthetic group binding, or catalysis. Site-directed mutagenesis was used to alter each of these residues, and differences in enzyme activity and substrate binding of the purified variants were analyzed. In addition, the effects of these replacements on the assembly and properties of the Mo cofactor and [4Fe-4S] centers were investigated using Mo and Fe determinations, coupled with electron paramagnetic resonance spectroscopy. The C148A, M149A, M306A, D163N, and R351Q variants were all inactive with either the physiological electron donor, reduced ferredoxin, or the nonphysiological electron donor, reduced methyl viologen, as the source of electrons, and all exhibited changes in the properties of the Mo cofactor. Charge-conserving D163E and R351K variants were also inactive, suggesting that specific amino acids are required at these two positions. The implications for the role of these five conserved active-site residues in light of these new results and previous structural, spectroscopic, and mutagenesis studies for related periplasmic nitrate reductases are discussed.

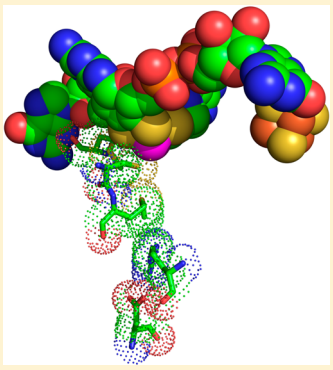

Nitrate assimilation in cyanobacteria[1,2] involves an initial two-electron reduction of nitrate to nitrite catalyzed by nitrate reductase, followed by the six-electron reduction of nitrite to ammonia and the subsequent incorporation of this ammonia to form glutamine. Although glutamine formation requires ATP, no redox chemistry is involved in this reaction. However, the next step in the pathway, in which one molecule of glutamine reacts with one molecule of 2-oxoglutarate to form two molecules of glutamate, involves a two-electron reduction.[1,2] In cyanobacteria, all three of the steps that involve a redox reaction utilize reduced ferredoxin (hereafter abbreviated as Fd) as the specific physiological electron donor.[1,2] In oxygenic photosynthetic eukaryotes, while Fd is the electron donor for both the reduction of nitrite to ammonia and of glutamine and 2-oxoglutarate to glutamate, the reduction of nitrate to nitrite utilizes reduced pyridine nucleotide as the reductant.[1,3]

The Fd-dependent nitrate reductase from *Synechococcus* sp. PCC 7942 (NarB) is one of the best characterized of these cyanobacterial nitrate reductases.[3] This soluble, monomeric enzyme has a molecular mass of approximately 78 kDa and contains a single [4Fe-4S] cluster and a single Mo bis-molybdopterin guanine dinucleotide cofactor (Moco) as its only prosthetic groups.[3] The oxidized $[4Fe\text{-}4S]^{2+}$ form of the iron−sulfur cluster is EPR silent, while one-electron reduction (E_m = −190 mV) produces a signal at 10 K characteristic of an $S = {}^1/_2$ $[4Fe\text{-}4S]^{+}$ cluster.[4,5] EPR spectra obtained at 60 K have been used to characterize the Mo center[4,5] and to determine an E_m value of −150 mV for a Mo(VI) to Mo(V) transition.[4] Previous work in our laboratory[5,6] demonstrated that the *Synechococcus* sp. PCC 7942 nitrate reductase forms a 1:1 complex with Fd ($K_d \sim 1-10\ \mu M$) at a low ionic strength. The fact that Fd can donate only a single electron and the fact that there is only a single high-affinity binding site on the enzyme for Fd lead to the conclusion that electrons enter the enzyme one at a time, one each from two separate reduced Fds, allowing the enzyme to collect the two electrons necessary for the reduction of nitrate to nitrite. This conclusion, which suggests that the two electrons that accumulate in the enzyme result in the reduction of Mo from the +6 to the +4 oxidation state, followed by the transfer of two electrons from the Mo(IV) species to nitrate, is consistent with results obtained by protein film voltammetry.[4]

An early study[3] used a combination of sequence alignments and site-directed mutagenesis to identify the four conserved cysteine residues in *Synechococcus* sp. PCC 7942, i.e., Cys9, Cys12, Cys16, and Cys56, that serve as ligands to the four Fe atoms of the [4Fe-4S] cluster. In this same study, sequence alignment considerations identified Cys148 as a likely ligand to

Received: May 8, 2015
Revised: August 21, 2015
Published: August 25, 2015

DOI: 10.1021/acs.biochem.5b00511
Biochemistry 2015, 54, 5557−5568

Mo, although no experimental data were presented to support this assignment. More recently, mutagenesis studies in our laboratories[5] presented evidence that three conserved basic amino acids, i.e., Lys58, Arg70, and Lys130, are essential for full catalytic activity and that a fourth conserved residue, Arg146, is not required for either activity or substrate binding. For both Lys58 and Arg70, the requirements are specific for the two amino acids present in the native enzyme, while at position 130, it is more likely that only a positively charged side chain is required.[5] The requirement for Lys58 appears to be related to its proximity to and its interaction with both of the two prosthetic groups.[5] In the case of Arg70 and Lys130, it has been shown that neither residue appears to be involved in substrate binding, but their exact roles in catalysis remain to be elucidated.

The *Synechococcus* sp. PCC 7942 nitrate reductase and other Fd-dependent cyanobacterial nitrate reductases are part of a large superfamily of Mo-containing enzymes that include both nitrate reductases and formate dehydrogenases.[7,8] The availability of three-dimensional structures of several of them,[9−17] along with sequence alignment analogies, not only identified Cys148 as a likely axial ligand for Mo in *Synechococcus* sp. PCC 7942 nitrate reductase but also suggested that Met149, Asp163, Met306, and Arg351 were likely to be located at or near the Moco active site of *Synechococcus* sp. PCC 7942 nitrate reductase. We have used site-directed mutagenesis coupled with activity assays, metal determinations, and EPR spectroscopy to demonstrate that each of these amino acids is essential for assembly of a wild-type Moco center and for full activity of *Synechococcus* sp. PCC 7942 nitrate reductase.

MATERIALS AND METHODS

Recombinant wild-type Fd from the cyanobacterium *Synechocystis* sp. PCC 6803 and a recombinant, His-tagged form of wild-type *Synechococcus* sp. PCC 7942 nitrate reductase were both expressed in *Escherichia coli* and purified as described previously.[5] Single-amino acid replacement variants of nitrate reductase were prepared by site-directed mutagenesis of the *narB* gene using the QuickChange (QC) site-directed mutagenesis kit (Stratagene) as described previously.[5] Site-specific replacement of the amino acids targeted for study was accomplished using a polymerase chain reaction (PCR) technique involving the mutagenic primers listed in Table 1. Expression of the mutated nitrate reductase variants in *E. coli* and purification of these variants were conducted using the same procedure used for the wild-type enzyme. SDS−PAGE analyses indicated that all of the proteins used in this study were at least 95% pure.

UV−visible absorbance spectra and difference absorbance spectra were obtained using a Shimadzu model UV-2401PC spectrophotometer, at a spectral resolution of 0.5 nm. Circular dichroism (CD) spectra, at a spectral resolution of 1.0 nm, were obtained using an OLIS model DSM-10 UV−vis CD spectrophotometer. Ferredoxin concentrations were measured from the absorbance at 420 nm, using an extinction coefficient of 9.7 mM^{-1} cm^{-1}.[18] Nitrate reductase concentrations were measured according to the method of Bradford,[19] using bovine serum albumin as a standard. X-Band (~9.6 GHz) EPR spectra were recorded for nitrate reductase samples as purified aerobically and reduced anaerobically with a 10-fold excess of dithionite, using a Bruker ESP-300E EPR spectrometer equipped with an ER-4116 dual-mode cavity and an Oxford Instruments ESR-9 flow cryostat. Spin quantifications were conducted under non-power saturation conditions using a 1 mM CuEDTA standard as described by Aasa and Vänngård.[20] The Fe and Mo contents were determined using inductively coupled plasma (ICP) mass spectrometry in the Department of Chemistry and Biochemistry at Arizona State University (Tempe, AZ) as described previously.[5]

Nitrate reductase activities, with either reduced methyl viologen (MV) or reduced ferredoxin as the electron donor, were measured as described previously.[5,6] All plots of nitrate reductase activity as a function of Fd concentration at saturating nitrate concentration and as a function of nitrate concentration at saturating Fd concentration gave excellent fits to the Michaelis−Menten equation. Kinetic parameters were calculated by fitting the data (i.e., initial velocity vs substrate concentration) to the Michaelis−Menten equation using GraphPad Prism 6. Formation of the complex between Fd and nitrate reductase was measured using the previously described spectral perturbation method,[5,6] except for the choice of the wavelength pairs used to monitor complex formation. Complex formation for wild-type nitrate reductase was monitored at 420 nm minus 600 nm. Variations were observed in the maxima of the difference spectrum, depending on the nitrate reductase variant, so to maximize the magnitude of the absorbance changes used for the K_d calculations, the following wavelength pairs were used to monitor ferredoxin binding by the variants: C148A, 470 nm minus 680 nm; M149A, 430 nm minus 520 nm; D163N: 400 nm minus 700 nm; D163E, 410 nm minus 460 nm; M306A, 410 nm minus 470 nm; R351Q, 460 nm minus 700 nm; R351K, 410 nm minus 490 nm. Complex formation for wild-type nitrate reductase with nitrate was monitored at 400 nm minus 470 nm. As was the case for complex formation with Fd, different wavelength pairs were used for the different variants to maximize the signal:noise ratio of the absorbance changes used to monitor complex formation: M149A, 350 nm minus 450 nm; D163N, 400 nm minus 680 nm; D163E, 460 nm minus 540 nm; M306A, 410 nm minus 470 nm; R351Q, 400 nm minus 700 nm; R351K, 410 nm minus 490 nm.

Table 1. Primers Used To Introduce Mutation into the pCSLM85 Nitrate Reductase Expression Plasmid[a]

primer name	sequence (5′−3′)
C148A_F	ACCAACTCGCGACTC**GCC**ATGTCCTCAGCGGTG
C148A_R	CACCGCTGAGGACAT**GGC**GAGTCGCGAGTTGGT
M149A_F	AACTCGCGACTCTGC**GCG**TCCTCAGCGGTGTCG
M149A_R	CGACACCGCTGAGGA**CGC**GCAGAGTCGCGAGTT
D163N_F	CTTTGCCTGGGTAGC**AAT**GGCCCACCCGCCTGC
D163N_R	GCAGGCGGGTGGGCC**ATT**GCTACCCAGGCAAAG
D163E_F	CTTTGCCTGGGTAGC**GAG**GGCCCACCCGCCTGC
D163E_R	GCAGGCGGGTGGGCC**CTC**GCTACCCAGGCAAAG
M306A_F	CTCTCGCTTTGGTCG**GCG**GGCGTCAATCAGTCG
M306A_R	CGACTGATTGACGCC**CGC**CGACCAAAGCGAGAG
R351Q_F	AACGCCATGGGCGGT**CAA**GAAACGGGTGGGCTC
R351Q_R	GAGCCCACCCGTTTC**TTG**ACCGCCCATGGCGTT
R351K_F	AACGCCATGGGCGGT**AAA**GAAACGGGTGGGCTC
R351K_R	GAGCCCACCCGTTTC**TTT**ACCGCCCATGGCGTT

[a]F indicates the forward direction primer, and R indicates the reverse direction primer. The mutagenic base replacements are highlighted in boldface.

DOI: 10.1021/acs.biochem.5b00511
Biochemistry 2015, 54, 5557−5568

RESULTS

Figure 1 shows the location, in the *in silico* model[5] previously developed for the *Synechococcus* sp. PCC 7942 nitrate reductase, of the five active-site amino acids selected for mutational replacement in this new study, i.e., Cys148, Met149, Asp163, Met306, and Arg351. The locations of the enzyme's prosthetic groups in this model are also shown in Figure 1. Table 2, indicates the distances, calculated using the *in silico* model of the enzyme, from these five amino acids to the Mo and to the nearest Fe of the [4Fe-4S] cluster. With the exception of Cys148, which corresponds in the sequence of *Synechococcus* sp. PCC 7942 nitrate reductase to the cysteine or selenocysteine that serves as an axial ligand to the Mo in related enzymes[8−17] and the nearby Met149 and Met306, none of the five amino acids are particularly close to the Mo and none of the five are very close to the [4Fe-4S] cluster.

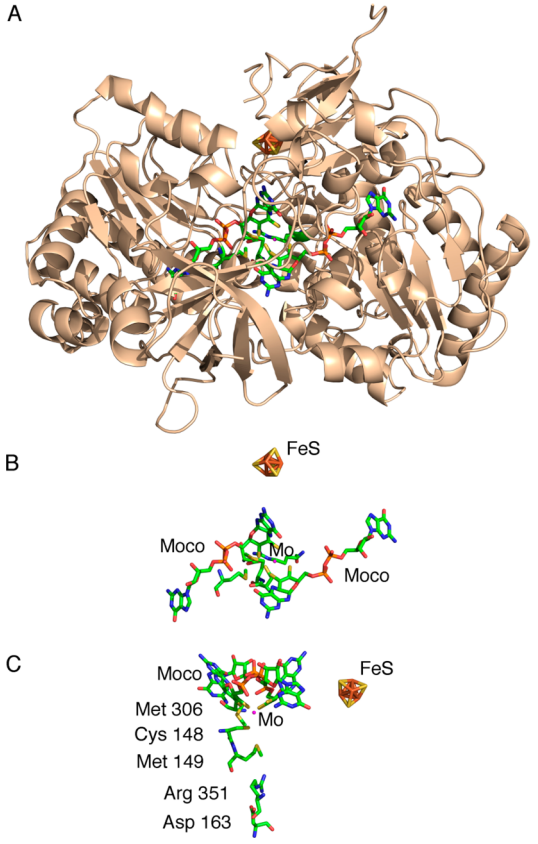

Figure 1. *In silico* model for the structure of *Synechococcus* sp. PCC 7942 nitrate reductase showing (A) the full model and the cofactors and selected residues (B) along the same view and (C) along a perpendicular view. The five residues targeted for mutagenesis are identified by their amino acid sequence numbers. The five side chains and cofactors are colored according to atom type. The Mo is represented as a purple dot.

Table 2. Distances from Amino Acid Residues Altered by Mutagenesis to the FeS Cluster and Mo Cofactor[a]

residue	distance to the Fe−S cluster (Å)	distance to Mo (Å)
C148	15.0	3.2
M149	14.1	7.3
M306	14.8	4.7
D163	20.4	14.2
R351	16.6	10.3

[a]The distances are measured from the end of each side chain to the closest point of each cofactor.

Before discussing the effect of mutagenic replacement of these five amino acids on the catalytic and substrate binding properties of the enzyme, we will summarize the Mo and Fe contents of all of the nitrate reductase samples used in this study (Table 3). The values obtained for the wild-type enzyme, i.e., 3.6 mol of Fe/mol of enzyme and 0.93 mol of Mo/mol of enzyme, agree with the theoretical predicted values of 4.0 and 1.0, respectively, within the experimental uncertainties of the measurements. Many of the substitutions characterized in this study have little significant effect on either the Mo or Fe contents. However, the replacement of Cys148 with alanine does produce a dramatic loss of Mo, consistent with the likelihood, based on comparisons between the amino acid sequences of *Synechococcus* sp. PCC 7942 nitrate reductase and related enzymes, that the thiol/thiolate of the side chain of Cys148 serves as a Mo ligand. Although neither our *in silico* model nor the known X-ray crystal structures for related enzymes[8−17] predict any direct interaction between the Mo and the [4Fe-4S] cluster, the C148A variant exhibits, in addition to the loss of Mo, a significantly lower level of [4Fe-4S] cluster than does the wild-type enzyme (Table 3). In contrast, as shown in Table 3, replacement of the nearby Met149 or Met306 with alanine has no effect on the content of either metal cofactor. Somewhat surprisingly, considering its distance from both Mo and Fe in our *in silico* model (see Table 2), and the distances to these metal centers from the corresponding amino acid in the structures of related enzymes,[8−17] the D163N variant exhibits significantly lower levels of Mo and of Fe than the wild-type enzyme does. In contrast, a charge-conserving replacement at this position, to produce a D163E variant, contained essentially wild-type levels of both Fe and Mo.

Circular dichroism (CD) spectroscopy was used to address the possibility that the effects of the mutational replacements conducted in this study on prosthetic group content, substrate binding affinities, or catalytic parameters result from large conformational changes. The CD spectra of all of the variants used in this study were measured in the ultraviolet region where α-helices and β-sheets show characteristic CD features. In fact, the CD spectra of all of the nitrate reductase variants examined in this study were very similar to those of the wild-type enzyme. Thus, although the possibility that these mutational substitutions produce small changes in conformation cannot be ruled out, we can conclude that none of them cause any major changes in secondary structure.

As shown in Table 3, replacement of Cys148, Met149, Asp163, Met306, or Arg351 produces enzyme variants that have lost all, or almost all, of their ability to catalyze the reduction of nitrate to nitrite, regardless of whether reduced Fd or reduced MV serves as the electron donor. No K_M values for either Fd or nitrate are shown for these variants, simply because the observed rates were far too low to allow these parameters to be estimated. It should be noted that the charge-conserving D163E variant does not have an activity significantly higher than that of the D163N variant, even though the D163N variant is significantly deficient in both Mo and Fe, while the D163E variant retains wild-type levels of Mo and Fe. These results indicate that the large loss of activity exhibited by the D163N variant cannot be attributed simply to loss of the cofactor and that there is a specific requirement for aspartate at

DOI: 10.1021/acs.biochem.5b00511
Biochemistry 2015, 54, 5557−5568

Table 3. Kinetic, Substrate Binding, and Prosthetic Group Contents of Nitrate Reductase Variants with Active-Site Replacements

enzyme	MV-linked specific activity[a]	Fd-linked specific activity[a]	iron[b]	molybdenum[b]	K_d nitrate (μM)	K_d ferredoxin (μM)
wild type	790 (100%)	30.5 (100%)	3.6 ± 0.45	0.93 ± 0.04	1.0 ± 0.3	7.8 ± 2.1
C148A	<0.2 (<0.1%)	<0.2 (<0.1%)	1.6 ± 0.10	0.38 ± 0.02	nd[c]	25.4 ± 14.6
M149A	4.9 (0.6%)	0.8 (2.6%)	3.8 ± 0.13	0.96 ± 0.03	3.1 ± 1.1	6.8 ± 1.3
D163N	15.6 (2.0%)	2.7 (8.8%)	2.4 ± 0.04	0.57 ± 0.01	32.2 ± 13.0	20.7 ± 11.3
D163E	20.4 (2.6%)	2.9 (9.5%)	3.9 ± 0.31	0.90 ± 0.10	1.2 ± 0.34	16.8 ± 2.6
M306A	5.8 (0.73%)	1.6 (5.2%)	3.9 ± 0.1	0.85 ± 0.02	39.5 ± 17.5	10.7 ± 6.8
R351Q	2.1 (0.3%)	1.9 (6.2%)	4.1 ± 0.08	0.95 ± 0.01	2.4 ± 0.9	11.5 ± 3.8
R351K	11.4 (1.4%)	3.5 (11.5%)	4.1 ± 0.37	1.13 ± 0.14	1 ± 0.3	1.4 ± 0.6

[a]In units of micromoles of nitrite produced per minute per milligram of enzyme. [b]In units of moles per mole of enzyme. [c]Could not be detected by spectral perturbations.

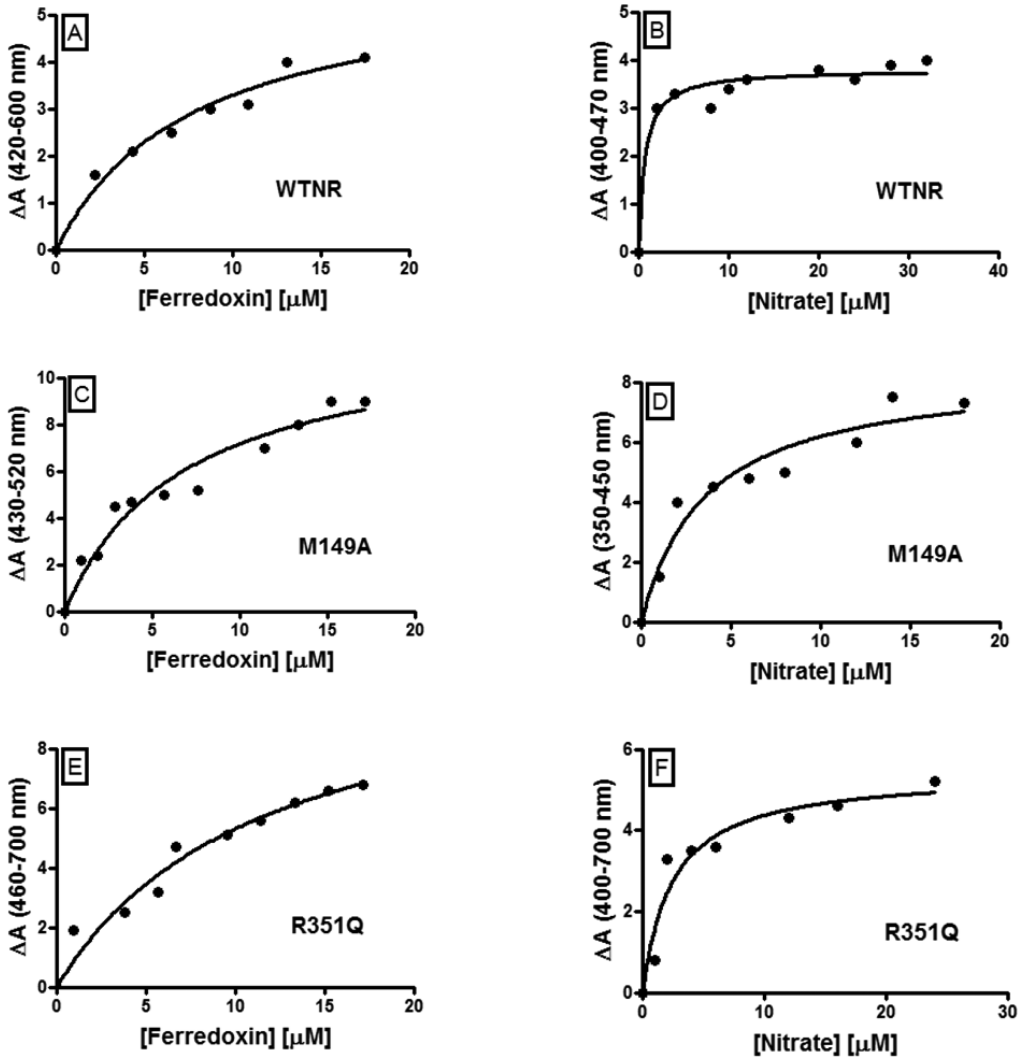

Figure 2. Measurement of substrate binding affinities by nitrate reductase variants. Titrations were conducted in samples containing 10 μM nitrate reductase in 25 mM HEPES buffer (pH 8.0). The wavelength pairs used to monitor complex formation are given in Materials and Methods.

position 163, rather than simply a requirement for a negatively charged side chain at this position. Similarly, the observation that the charge-conserving R351K variant does not have an activity significantly higher than that of the R351Q variant that eliminates the positive charge on the side chain suggests that there is a specific requirement for arginine at position 351, rather than there being simply a requirement for a positive charge at this position.

In principle, the losses of activity for the variants described above might have resulted from large decreases in substrate binding affinities. Fortunately, spectral perturbations that result from formation of a complex between the enzyme and both Fd and nitrate make it possible to measure these affinities directly.[5,6] Figure 2 shows the results of representative substrate binding data for the wild-type enzyme and two of the variants produced for this study. Replacement of amino acids at these

DOI: 10.1021/acs.biochem.5b00511
Biochemistry 2015, 54, 5557−5568

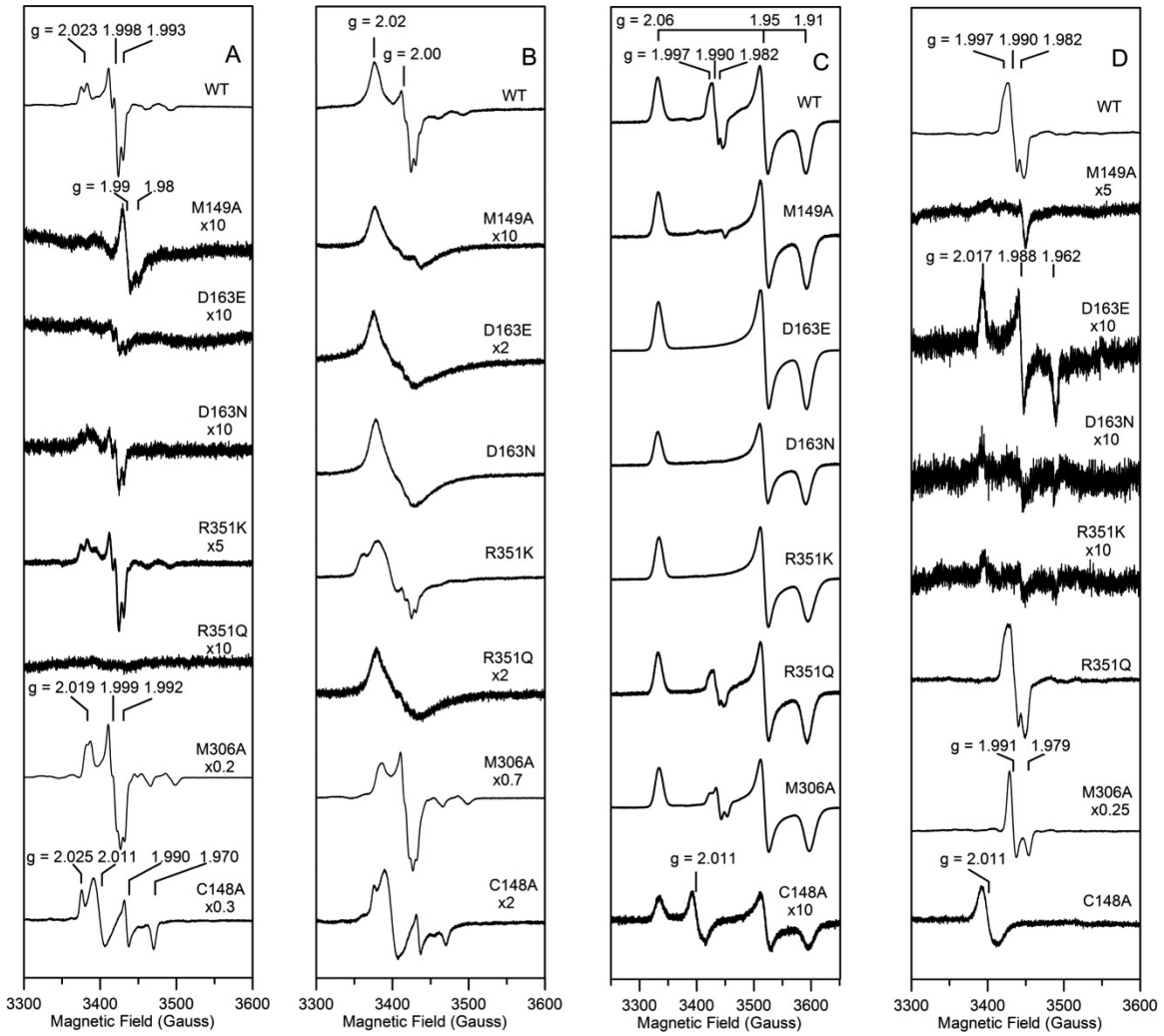

Figure 3. EPR spectra of wild-type *Synechococcus* sp. PCC 7942 nitrate reductase and the M149A, D163E, D163N, R351K, R315Q, M306A, and C148A variants. (A) Spectra of air-oxidized samples recorded at 70 K and a microwave power of 2 mW. (B) Spectra of air-oxidized samples recorded at 10 K and a microwave power of 2 mW. (C) Spectra of dithionite-reduced samples recorded at 20 K and a microwave power of 1 mW. (D) Spectra of dithionite-reduced samples recorded at 70 K and a microwave power of 2 mW. Protein concentrations for the samples ranged from 0.22 to 0.65 mM, and the buffering medium consisted of 25 mM HEPES with 200 mM NaCl and 100 μM sodium molybdate. All spectra were recorded at 9.60 GHz and a modulation amplitude of 6.3 G, and the intensities have been normalized with respect to the wild-type enzyme, to correct for differences in spectrometer gain and sample protein concentration.

five positions putatively at or near the active site of the enzyme produces relatively modest changes in binding affinities for Fd and nitrate (i.e., a <5-fold decrease in affinity), with the exceptions of the large decreases in affinity for nitrate exhibited by the D163N and M306A variants (as no spectral perturbations were observed when the C148A variant was titrated with nitrate, we are not currently able to determine whether this amino acid replacement affects the affinity of the enzyme for nitrate). It should also be noted that in the case of the charge-conserving variant, D163E, even though its activity is essentially as low as that of the D163N variant, its binding affinities for its two substrates are closer to those measured for the wild-type enzyme. Given that both of the substrates, i.e., Fd and nitrate, carry net negative charge, the observation that a negatively charged side chain at position 163 increases enzyme affinity for both substrates is counterintuitive. In contrast, elimination of the positive charge at position 351 has little or no effect on the binding affinity for either Fd or nitrate. The most dramatic effect of these replacements on substrate binding is the almost 40-fold decrease for nitrate observed with the M306A variant, a change that occurs with little effect on the binding affinity for Fd.

EPR spectroscopy has proven to be a powerful tool for characterizing both the Mo and iron−sulfur cluster prosthetic groups of nitrate reductases and related enzymes.[4,5,7,14,21] Figure 3 compares the X-band spectra of wild-type *Synechococcus* sp. PCC 7942 nitrate reductase with those of variants involving putative residues involved in interacting with or channeling substrates to Moco, i.e., M149A, D163E, D163N, R351K, R351Q, M306A, and C148A. Figures 4 and 5 show high-resolution spectra of selected air-oxidized and dithionite-reduced Mo(V) species, respectively, which reveal resolved proton hyperfine and $^{95/97}$Mo satellite spectra ($I = {}^5/_2$; 25% natural abundance). EPR studies at 70 K were used to selectively investigate $S = {}^1/_2$ Mo(V) species that, in contrast to fast-relaxing $S = {}^1/_2$ $[3Fe\text{-}4S]^+$ and $[4Fe\text{-}4S]^+$ clusters that are clearly observable only below 30 K, exhibit slow relaxation and consequently are readily observed without broadening at 70 K.

DOI: 10.1021/acs.biochem.5b00511
Biochemistry 2015, 54, 5557−5568

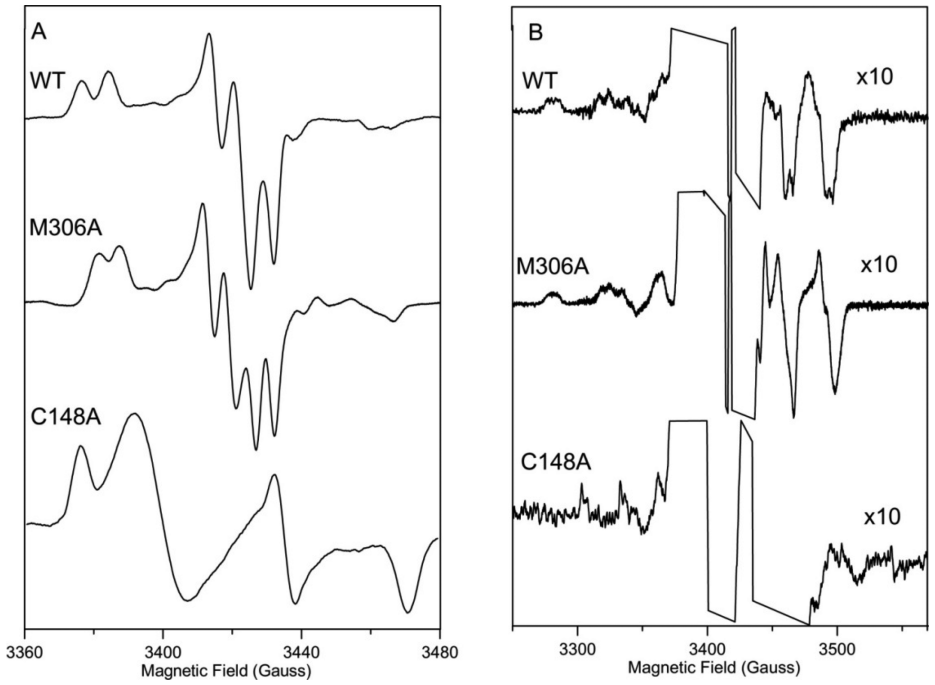

Figure 4. High-resolution EPR spectra of air-oxidized WT, M306A, and C148A *Synechococcus* sp. PCC 7942 nitrate reductase. Spectra were recorded at 70 K and a microwave power of 2 mW, with a microwave frequency of 9.60 GHz and a modulation amplitude of 2.9 G. (A) Spectra showing proton-split Mo(V) resonances for WT ($g_{1,2,3}$ = 2.023, 1.998, and 1.993, and $A_{1,2,3}$ = 6.8, 7.5, and 6.8 G) and M306A variant ($g_{1,2,3}$ = 2.019, 1.999, and 1.992, and $A_{1,2,3}$ = 5.6, 5.6, and 5.3 G), and the lack of any resolvable proton splitting on the rhombic Mo(V) resonance ($g_{1,2,3}$ = 2.025, 1.990, and 1.970) observed for the C148A variant. (B) Broad scans of the same spectra shown in panel A with 10-fold amplification to show the Mo-satellite hyperfine resulting from the 25% natural abundance of $I = {}^{5}/_{2}$ ^{95}Mo and ^{97}Mo isotopes. The observation of Mo satellites confirms the assignment of these resonances as Mo(V) species.

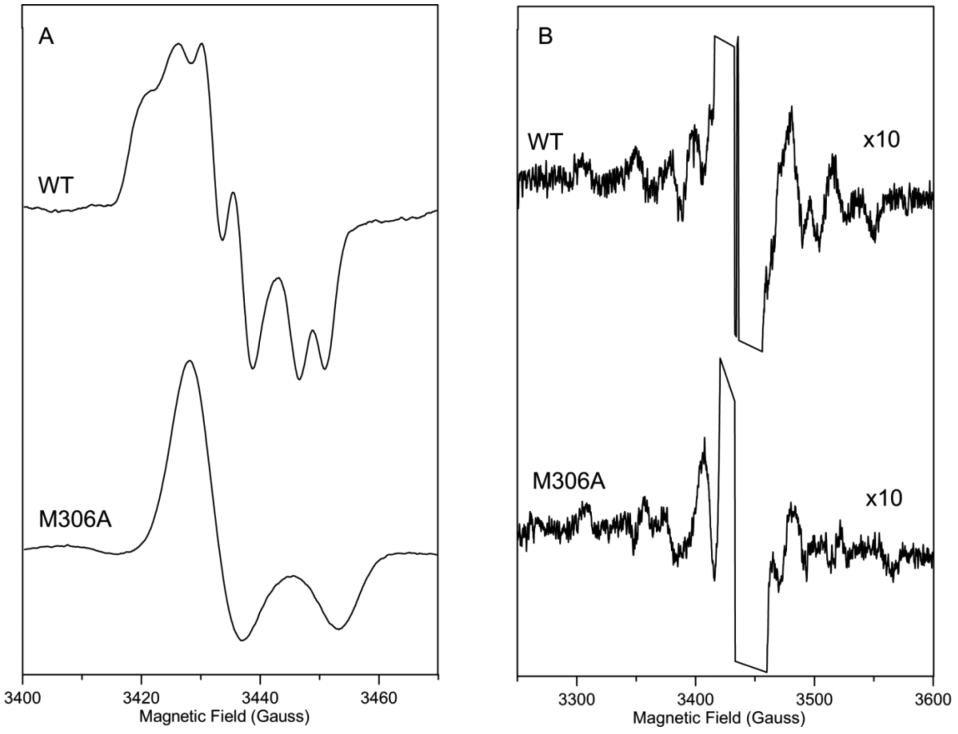

Figure 5. High-resolution EPR spectra of dithionite-reduced WT and M306A *Synechococcus* sp. PCC 7942 nitrate reductase. Spectra were recorded at 70 K and a microwave power of 2 mW, with a microwave frequency of 9.60 GHz and a modulation amplitude of 2.9 G. (A) Spectra showing the proton-split Mo(V) resonances for WT ($g_{1,2,3}$ = 1.997, 1.990, and 1.982, and $A_{1,2,3}$ = 6.5, 6.0, and 5.0 G) and the lack of any resolvable proton splitting on the axial Mo(V) resonance ($g_{\perp}$ = 1.991, and $g_{\parallel}$ = 1.979) observed for the M306A variant. (B) Broad scans of the same spectra shown in panel A with 10-fold amplification to show the Mo-satellite hyperfine resulting from the 25% natural abundance of $I = {}^{5}/_{2}$ ^{95}Mo and ^{97}Mo isotopes. The observation of Mo satellites confirms the assignment of these resonances as Mo(V) species.

DOI: 10.1021/acs.biochem.5b00511
Biochemistry 2015, 54, 5557−5568

Table 4. EPR Parameters and Spin Quantifications for Mo(V) and [4Fe-4S]$^{+}$ Centers in Wild-Type and Variant Forms of *Synechococcus* sp. PCC 7942 Nitrate Reductase

	aerobically purified Mo(V) resonance[a]			dithionite-reduced Mo(V) resonance[a]			dithionite-reduced [4Fe-4S]$^{+}$ resonance[b]	
sample	name	$g_{1,2,3}$ [$A_{1,2,3}$ (G)]	spin/mole[c]	name	$g_{1,2,3}$ [$A_{1,2,3}$ (G)]	spin/mole[c]	$g_{1,2,3}$	spin/mole[c]
wild type	very high-*g*	2.023, 1.998, 1.993 (6.8, 7.5, 6.8)	0.23	high-*g* split	1.997, 1.990, 1.982 (6.5, 6.0, 5.0)	0.19	2.058, 1.951, 1.908	0.95
M149A		1.99, 1.99, 1.98	0.02		none		2.058, 1.951, 1.908	0.91
D163E	very high-*g*	2.023, 1.998, 1.993 (6.8, 7.5, 6.8)	0.004	low-potential	2.017, 1.988, 1.962	0.08	2.058, 1.951, 1.908	1.02
D163N	very high-*g*	2.023, 1.998, 1.993 (6.8, 7.5, 6.8)	0.01	low-potential	2.017, 1.988, 1.962	0.02	2.058, 1.951, 1.908	0.59
R351K	very high-*g*	2.023, 1.998, 1.993 (6.8, 7.5, 6.8)	0.03	low-potential	2.017, 1.988, 1.962	0.01	2.058, 1.951, 1.908	0.86
R351Q		none		high-*g* split	1.997, 1.990, 1.982 (6.5, 6.0, 5.0)	0.20	2.058, 1.951, 1.908	0.87
M306A	very high-*g*	2.019, 1.999, 1.992 (5.6, 5.6, 5.3)	0.85	high-*g* unsplit	1.991, 1.991, 1.979	0.83	2.058, 1.951, 1.908	0.85
C148A		2.025, 1.990, 1.970	0.39		none		2.058, 1.951, 1.908	0.04

[a]70 K and 2 mW; [b]10 K and 1 mW; [c]Values of spin/mole are accurate to ±10%.

At 70 K, air-oxidized samples of the wild-type enzyme exhibit the "very high-*g*" proton-split $S = {}^{1}/_{2}$ Mo(V) resonance ($g_{1,2,3}$ = 2.023, 1.998, and 1.993, g_{av} = 2.005, and $A_{1,2,3}$ = 6.8, 7.5, and 6.8 G), accounting for 20−30% of the Mo content, that has previously been reported for *Synechococcus* NarB[4,5] (see Figures 3A and 4 and Table 4). This Mo(V) resonance persists, albeit somewhat broadened, at 10 K and 2 mW and is overlapped by a broad fast-relaxing resonance with a $g_{\parallel} \sim 2.02$ and $g_{\perp} \sim 2.00$ characteristic of an $S = {}^{1}/_{2}$ cubane-type [3Fe-4S]$^{+}$ cluster, accounting for <10% of the Fe content, that is formed by partial O_2-induced degradation of the native [4Fe-4S]$^{2+}$ cluster[5] (see Figure 3B). After dithionite reduction, the 10 K spectra of the wild-type enzyme exhibit the characteristic fast-relaxing rhombic resonance ($g_{1,2,3}$ = 2.058, 1.951, and 1.908) associated with the $S = {}^{1}/_{2}$ [4Fe-4S]$^{+}$ cluster in reduced *Synechococcus* NarB[4,5] (see Figure 3C and Table 4). The resonance accounts for 90−100% of the Fe content, suggesting that some or all of the [3Fe-4S]$^{+}$ clusters reconvert to [4Fe-4S]$^{+}$ clusters upon dithionite reduction, by incorporating adventitious Fe(II) into reduced [3Fe-4S]^{0} clusters, as is frequently observed with [3Fe-4S]$^{+}$ clusters generated by O_2-induced degradation of [4Fe-4S]$^{2+}$ clusters.[22] Previous EPR studies of wild-type *Synechococcus* NarB have revealed two distinct types of Mo(V) resonances in dithionite-reduced samples that can be observed along with the [4Fe-4S]$^{+}$ resonance at 20 K and in isolation at 70 K.[4,5] One is termed the "high-*g*" proton-split Mo(V) signal ($g_{1,2,3}$ = 1.997, 1.990, and 1.982, g_{av} = 1.990, and $A_{1,2,3}$ = 6.5, 6.0, and 5.0 G) that accounts for ∼20% of the Mo content.[4] The other is a weak rhombic resonance ($g_{1,2,3}$ = 2.017, 1.988, 1.962, g_{av} = 1.989) with negligible proton splitting, accounting for <10% of the Mo content.[5] Analogous resonances, termed the "low-potential" Mo(V) resonance, have been observed in dithionite-reduced bacterial assimilatory nitrate reductases.[16,23] In our hands, different purifications of dithionite-reduced wild-type *Synechococcus* NarB exhibit one of these two signals or the other, and we have yet to define specific experimental conditions for generating each type of Mo(V) resonance. As shown in Figures 3D and 5 and Table 4, the dithionite-reduced wild-type enzyme used in this work exhibits the "high-*g*" proton-split Mo(V) signal accounting for ∼20% of the Mo content. The proton hyperfine in the "high-*g*" proton-split Mo(V) signal shown in Figure 3D is not resolved because of high modulation amplitudes (6.3 G) but is clearly seen, along with the $^{95/97}$Mo satellites, in spectra recorded with lower modulation amplitudes (2.9 G) (see Figure 5).

Only the C148A mutation has a significant effect on the EPR properties of the [4Fe-4S]$^{+}$ cluster in dithionite-reduced samples (see Figure 3C and Table 4). However, the difference relates only to the intensity of the resonance, 10% of the [4Fe-4S] clusters in the C148A variant and 4% of total wild-type [4Fe-4S] cluster content based on EPR spin quantifications and Fe determinations (see Tables 3 and 4). This may result from a lower reduction potential for the [4Fe-4S]$^{2+}$ center in the C148A variant, coupled with the mutation having an effect on the assembly or stability of the [4Fe-4S] cluster. Significantly, the C148A mutation does not affect the *g* values of the rhombic $S = {}^{1}/_{2}$ [4Fe-4S]$^{+}$ resonance, and there is no evidence of $S = {}^{3}/_{2}$ [4Fe-4S]$^{+}$ in the low-field region.

In contrast, all the mutations involving the putative active residues result in significant perturbations of air-oxidized and/or dithionite-reduced Mo(V) resonances compared to those of the wild-type enzyme. The air-oxidized D163E, D163N, and R351K variants exhibit "very high-*g*" proton-split $S = {}^{1}/_{2}$ Mo(V) resonances, albeit with intensities that are 50-, 25-, and 7-fold lower, respectively, than that of the wild-type enzyme (see Figure 3A and Table 4). The lower intensities of the Mo(V) resonances in these variants facilitate observation of the shape of the $S = {}^{1}/_{2}$, $g_{\parallel} \sim 2.02$ and $g_{\perp} \sim 2.00$ [3Fe-4S]$^{+}$ resonances in the 10 K spectra of D163E and D163N (see Figure 3B). The dithionite-reduced samples of these variants also exhibit weak "low-potential" Mo(V) signals, albeit with inverted intensities, i.e., R351K being the weakest and D163E the strongest (see Figure 3D). This suggests that these mutations produce environmental perturbations that change the Mo(IV)/Mo(V) and/or Mo(V)/Mo(VI) redox potentials without changing the Mo coordination environment. A similar conclusion can be drawn for the R351Q variant, which exhibits no Mo(V) resonance in the air-oxidized form at 70 K and a wild-type-like "high-*g*" proton-split Mo(V) signal in the dithionite-reduced form at 70 K (see Figure 3A,D and Table 4).

More distinct changes in the EPR properties of the Mo(V) centers are observed for the M149A, M306A, and C148A variants. Despite almost stoichiometric Mo content (see Table 3), the M149A variant exhibits an anomalous and very weak $S = {}^{1}/_{2}$ axial resonance ($g_{\perp} \sim 1.99$, and $g_{\parallel} \sim 1.98$) that is attributed

DOI: 10.1021/acs.biochem.5b00511
Biochemistry 2015, 54, 5557−5568

to a Mo(V) species and accounts for <2% of the Mo content in the air-oxidized form at 70 K (see Figure 3A and Table 4). Upon dithionite reduction, no significant Mo(V) signals are observed at 10 or 70 K (see Figure 3C,D). Hence, either the Mo center is not redox active, or the Mo(VI)/Mo(V) and Mo(V)/Mo(IV) redox potentials do not permit observation of significant Mo(V) species in air-oxidized or dithionite-reduced samples. Regardless, the M149A mutation clearly has had a major effect on the redox properties and/or ligation of the Mo center. For the air-oxidized M306A variant, the "very high-g" proton-split $S = {}^1/_2$ Mo(V) resonance ($g_{1,2,3}$ = 2.019, 1.999, and 1.992, g_{av} = 2.003, and $A_{1,2,3}$ = 5.6, 5.6, and 5.3 G) is significantly perturbed compared to that of the wild-type enzyme ($g_{1,2,3}$ = 2.023, 1.998, and 1.993, g_{av} = 2.005, and $A_{1,2,3}$ = 6.8, 7.5, and 6.8 G) and accounts for ∼100% of the Mo concentration compared to 20% for the wild-type enzyme (see Figures 3A and 4 and Table 4). Likewise, the dithionite-reduced M306A variant exhibits a perturbed axial "high-g" Mo(V) signal ($g_\perp$ = 1.991, $g_\parallel$ = 1.979, and g_{av} = 1.987, with no resolvable proton hyperfine) compared to that of the wild type ($g_{1,2,3}$ = 1.997, 1.990, and 1.982, g_{av} = 1.990, and $A_{1,2,3}$ = 6.5, 6.0, and 5.0 G for the proton hyperfine), accounting for ∼100% of the Mo concentration compared to 20% for the wild-type enzyme (see Figures 3D and 5 and Table 4). In accord with the putative role of C148 as a Mo ligand, the most dramatic changes in the Mo(V) EPR properties were observed in the C148A variant. The air-oxidized sample exhibited a new type of rhombic Mo(V) signal ($g_{1,2,3}$ = 2.025, 1.990, and 1.970, and g_{av} = 1.995, with no resolvable proton hyperfine), accounting for 100% of the Mo concentration (see Figures 3A and 4 and Tables 3 and 4). No Mo(V) signals were observed in the dithionite-reduced sample (see Figure 3). The observation of "Mo satellites" due to the 25% natural abundance of $I = {}^5/_2$ ^{95}Mo and ^{97}Mo isotopes unambiguously identifies the sharp rhombic resonance in the air-oxidized sample as originating from Mo(V) (see Figure 4). All four of the EPR spectra recorded for the C148A variant exhibited a slow-relaxing and broad near-isotropic resonance centered at 2.01 (see Figure 3). This is tentatively attributed to a radical species.

In summary, EPR studies of the putative active-site variants indicate that each of them perturbs the Mo(V) EPR signals, suggesting that C148, M149, D163, R351, and M306 all change the environment and redox properties of the Moco site to some extent. EPR-monitored redox titrations would clearly be helpful in clarifying the redox properties of the Moco in these mutants. However, the weakness of the Mo(V) EPR signals observed for the majority of these mutants makes such meaurements particularly challenging. Significantly, the most dramatic changes in the Mo(V) signals are observed for the residues closest to the Mo, i.e., M149, M306, and C148 (see Table 2), and the marked changes in the Mo(V) EPR signals associated with the C148A variant are consistent with loss of C148 as a Mo ligand. Moreover, both the EPR studies and Fe determinations indicate that the loss of this Mo ligand also affects the ability of the enzyme to assemble or stabilize the [4Fe-4S] cluster.

DISCUSSION

A combination of *in silico* modeling of a possible structure for *Synechococcus* sp. PCC 7942 nitrate reductase and comparisons of the amino acid sequence of this cyanobacterial nitrate reductase to those of related enzymes identified Cys148, Met149, Asp163, M306, and Arg351 as being likely to play important roles in the catalytic mechanism of the enzyme. The results presented above, using a mutagenic replacement approach, provide direct support for the hypothesis that all five of these amino acids are in fact essential for catalytic activity. The observation that variants with replacements at all five of these positions are equally inactive, regardless of whether Fd or MV is used as the electron donor, suggests that these amino acids are not involved in binding and/or properly orienting Fd but rather are involved in some other aspect of the catalytic cycle.

Before discussing the implications of the results for specific variants, we start by summarizing the current picture that has emerged for the catalytic mechanism and active-site structures, based on the available structural, electrochemical, and spectroscopic data for the closely related soluble cytoplasmic assimilatory nitrate reductases, such as *Synechococcus* NarB and soluble periplasmic dissimilatory nitrate reductases, such as the monomeric *Desulfovibrio desulfuricans* NapA or the A subunit of the heterodimeric NapAB enzymes from *Paracoccus pantotrophus*, *E. coli*, *Rhodobacter sphaeroides*, and *Cupriavidus necator*. In common with other members of the DMSO reductase family of molybdoenzymes, which have Mo bis-molybdopterin cofactors and cycle between the Mo(IV/V/VI) oxidation states, structural and spectroscopic studies of as purified soluble nitrate reductases have revealed significant heterogeneity in Mo coordination[12,16,17,21] and demonstrated that reductive activation is required to obtain homogeneous samples and optimal activity.[21,24,25] However, upon irreversible reduction to the functional Mo(IV) form, there is as yet no evidence of a functional EPR-active Mo(V) intermediate, when periplasmic dissimilatory nitrate reductases undergo redox cycling between the EPR-silent Mo(IV) and Mo(VI) forms, in the presence or absence of substrate.[24] This may be a consequence of a very transient Mo(V) intermediate and/or very similar Mo(IV/V) and Mo(V/VI) redox potentials. Nevertheless, as discussed below, both the very high-g and high-g Mo(V) EPR species, which are observed in NarB and related nitrate reductases,[21] appear to be oxidized precursors of the functional form, and recent evidence suggests that the Mo coordination in the high-g Mo(V) species is likely to be closely related to a functional Mo(V) form.[25]

Three distinct Mo(V) EPR signals have been observed in wild-type *Synechococcus* NarB: very high-g in aerobically purified samples and high-g or low-potential in dithionite-reduced samples (see Figure 4 and Table 4). The type of signal present in dithionite-reduced samples is preparation-dependent,[4,5] again illustrating the plasticity of the Moco in these enzymes, but only the high-g signal, reported by Jepson et al.,[4] was observed in this work. Redox titrations indicated that the high-g Mo(V) species accounts for ∼100% of the Mo content at −280 mV and persists with no significant decrease in intensity down to −550 mV.[4] In our studies of aerobically prepared NarB, the very high-g Mo(V) species accounted for ∼20% of the Mo content and showed near stoichiometric conversion from the very high-g to the high-g signal upon dithionite reduction (see Table 4). Moreover, the return of the very high-g signal following exposure to air suggests a reversible redox interconversion between these two species.[4] This is consistent with the MoS_6 structures that have been proposed on the basis of the most recent crystal structures[16,17] and theoretical analysis of the EPR parameters using DFT calculations[26] (see Figure 6). The high-g Mo(V) structure is essentially trigonal prismatic involving six sulfur ligands: two dithiolenes from the MGDs

DOI: 10.1021/acs.biochem.5b00511
Biochemistry 2015, 54, 5557−5568

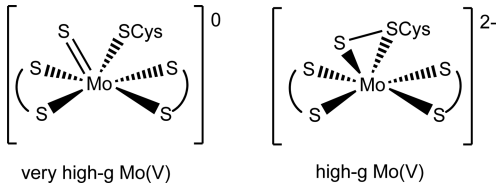

Figure 6. Proposed schematic structures for the very high-*g* and high-*g* Mo(V) species.[23]

and a side-on η^2 cysteine disulfide with a partial disulfide bond. Two-electron oxidation results in cleavage of the partial disulfide bond to yield terminal sulfido and cysteinate ligands in the very high-*g* Mo(V) structure. In both cases, the nonexchangeable proton hyperfine splittings are attributed to the β-CH_2 protons of the coordinated cysteine.[26,27] This suggests that the cysteine ligand is dissociated in the rhombic low-potential Mo(V) species, which lacks proton hyperfine coupling and is observed in some samples of dithionite-reduced wild-type NarB and *D. desulfuricans* NapA.[16,23] Alternatively, the low-potential Mo(V) species could correspond to a form with a terminal cysteine persulfide ligand, which would be expected to exhibit much weaker cysteine β-CH_2 proton hyperfine coupling. However, the low-potential Mo(V) species is always a minor species (<10% of the Mo content[5]), and it remains to be seen if it corresponds to a catalytically relevant Mo(V) species.

In addition to the intricate interplay of Mo- and sulfur ligand-based redox chemistry, the reductive activation process in periplasmic nitrate reductases has recently been proposed to involve molybdopterin-based redox chemistry.[25] The need for reductive activation before steady state catalysis can be observed was first demonstrated by Butt et al. in protein film voltammetry (PFV) of *P. pantotrophus* respiratory nitrate reductase (NarGH) and *Synechococcus* NarB.[24] Subsequent EPR and PFV studies of *R. sphaeroides* NapAB demonstrated that reductive activation is irreversible, occurs in the absence of substrate, and quantitatively correlates with the loss of the high-*g* Mo(V) EPR signal in a reaction that is too slow to be part of the normal catalytic cycle.[21] More detailed kinetic studies of *R. sphaeroides* NapAB using room-temperature EPR and direct electrochemistry revealed that reductive activation occurs prior to Mo reduction and involves changes in the exchange coupling between Mo(V) and the $[4Fe\text{-}4S]^+$ cluster without significant coordination changes at the Mo(V) center.[25] On the basis of the known molybdopterin redox chemistry, this was interpreted in terms of slow cyclization of the pyran ring and irreversible two-electron two-proton reduction of the oxidized dihydromolybdopterin to yield the catalytically competent tricyclic tetrahydromolybdopterin proximal to the [4Fe-4S] cluster.[25] This slow rate-limiting transformation precedes rapid reduction to the Mo(IV) state, which calculations indicate would weaken the Mo−S(Cys) bond, thereby facilitating nitrate binding and enzyme turnover by a sulfur shift-type mechanism.[25,28]

While a slow reductive activation step involving molybdopterin-based redox chemistry is an attractive proposal that explains the spectroscopic and redox properties of periplasmic nitrate reductases,[21,25] it has yet to be confirmed by high-resolution crystallographic data. However, the available data suggest it may not apply to the assimilatory *Synechococcus* NarB,[4] which uses a much lower-potential electron donor ($[2Fe\text{-}2S]^{2+/+}$ Fd, $E_m \sim -400$ mV, compared to ubiquinone/ubiquinol, $E_m \sim 60$ mV, or menaquinone/menaquinol, $E_m \sim -80$ mV, for periplasmic nitrate reductases) and has a much lower electrode potential for optimal activity based on PFV studies (approximately −450 mV for NarB, compared to approximately −100 mV for periplasmic nitrate reductases).[4] Moreover, the observation that NarB activity is turned on at potentials below −200 mV, where the cofactors correspond predominantly to the $[4Fe\text{-}4S]^+$ and high-*g* Mo(V) species that both increase to become stoichiometric and then persist as the potential is lowered to −550 mV,[4] has led to the proposal that nitrate binds to the high-*g* Mo(V), which increases the Mo(V)/(IV) redox potential, thereby allowing the $[4Fe\text{-}4S]^+$ cluster to effect reduction to the Mo(IV) state.[4]

Crystallographic data for periplasmic nitrate reductases indicate that the transfer of an electron from the $[4Fe\text{-}4S]^+$ cluster to the proximal MGD is mediated by the amido group of a conserved lysine (Lys58 in NarB) that interacts with the [4Fe-4S] cluster and the terminal amido group of tetrahydromolybdopterin.[17] Notably, site-directed mutations of Lys58 in NarB (K58Q and K58R) result in a complete loss of activity, low Fe contents, negligible $[4Fe\text{-}4S]^+$ resonances in dithionite-reduced samples, and negligible Mo(V) resonances in air-oxidized and dithionite-reduced samples,[5] suggesting that this residue is essential for [4Fe-4S] cluster stability and/or assembly.

Previous mutagenesis studies of the active-site cysteine in the periplasmic dissimilatory nitrate reductase (Nap) from *Ralstonia eutropha* reported complete loss of activity for a C181S variant.[29] The data presented herein for mutation of the equivalent cysteine (C148A) in NarB, i.e., complete loss of activity, low Mo and Fe content, and major perturbations of the EPR-active Mo(V) forms, clearly support the hypothesis that it also serves as a ligand to the Mo in cytoplasmic assimilatory nitrate reductases, a role that had previously been crystallographically documented for the corresponding cysteine (or selenocysteine) in related enzymes.[9−17] In particular, the lack of proton hyperfine coupling on the rhombic Mo(V) resonance that accounts for all the Mo in air-oxidized samples of the C148A variant supports the view that the hyperfine coupling originates from the cysteine β-CH_2 protons and hence is diagnostic of loss of the cysteine ligand. The fact that no UV-visible spectral perturbations occurred when nitrate was added to the C148A variant of the enzyme (see Table 3), although not definitively proving that this variant is incapable of binding nitrate with reasonable affinity, is certainly consistent with the proposed role for this cysteine residue in facilitating productive nitrate binding. In addition, the loss of this Mo ligand also affects the ability of the enzyme to assemble or stabilize the [4Fe-4S] cluster. Arsenite oxidase is currently the only member of the bis-molybdopterin DMSO reductase family that does not contain a covalent linkage to Mo in the form of serine, cysteine, or selenocysteine.[30] The corresponding residue in arsenite oxidase is an alanine that is contained in a loop that is folded away from the Mo, creating an active site more exposed than those of other members of the DMSO reductase family.[30] However, the NarB C148A variant shows no spectroscopic similarity to arsenite oxidase, which is proposed to catalytically cycle between dioxo-Mo(VI) and monooxo-Mo(IV) redox states at high redox potentials (292 mV vs SHE at pH 5.9), without any significant accumulation of Mo(V) species.[31,32]

Met149 in the *Synechococcus* NarB corresponds to Met141 in *D. desulfuricans* Nap, the structure of which[10] was used as the basis for our *in silico* modeling of the *Synechococcus* enzyme.[5] This methionine is highly conserved in periplasmic nitrate

DOI: 10.1021/acs.biochem.5b00511
Biochemistry 2015, 54, 5557−5568

reductases, with the sulfur positioned 6−8 Å from the Mo, and has been proposed to function as part of a solvent-accessible channel involved in "guiding" nitrate to the active site in the *D. desulfuricans* enzyme.[16] Previous mutagenesis studies involving the equivalent methionine in other organisms have been contradictory with respect to the effect on enzyme activity but generally provide support for roles in channeling nitrate to Mo and modulating the Mo and [4Fe-4S] cluster redox chemistry.[15,29,33] The M182H variant in *Ra. eutropha* Nap was found to be completely inactive.[29] In contrast, the M153A variant of *R. sphaeroides* NapAB exhibited wild-type activity using methyl viologen as the electron donor, but did result in an 8-fold increase in the K_m for nitrate binding.[15] In addition, the high-*g* Mo(V) signal that can be observed in the wild-type enzyme over a wide range of potentials (from 570 to −225 mV), in addition to a weak very high-*g* Mo(V) signal, was replaced with a very weak rhombic resonance ($g_{1,2,3}$ = 1.992, 1.982, and 1.973, with no resolved proton hyperfine coupling), maximally accounting for 0.03 spin/[4Fe-4S] cluster and observable between 0 and 200 mV.[15,33] The midpoint potential of the $[4Fe\text{-}4S]^{2+,+}$ cluster was also shifted by ∼100 mV to the negative compared to its value in the wild-type enzyme. In contrast to the M153A variant of *R. sphaeroides* NapAB, the M149A variant of *Synechococcus* NarB results in greatly reduced activity [0.6 and 2.6% of that of the wild type, using MV and Fd as electron donors, respectively (see Table 3)]. However, the modest effect on the affinity of NarB for binding nitrate [3-fold increase in K_d (see Table 3)] is in accord with the small decrease in nitrate binding ability observed for the M153A variant of *R. sphaeroides* NapAB and is consistent with the hypothesis that the side chain of this methionine may be involved in efficiently guiding nitrate toward the active site at a rate compatible with enzyme turnover, but that it is not involved in the final binding of nitrate at the active site. The EPR changes for M149A NarB are also very similar to those reported for the M153A variant of *R. sphaeroides* NapAB,[15,33] i.e., loss of both the very high-*g* and high-*g* Mo(V) signals and the appearance at high potentials of a very weak resonance ($g_{1,2,3}$ ∼ 1 0.99, 1.99, and 1.98, with no resolved proton hyperfine coupling, accounting for 0.02 spin/mol). Hence, we attribute the loss of activity associated with the M149A mutation to major changes in the redox properties and/or ligation of the Mo center. The marked discrepancy in the activity of the M153A variant of *R. sphaeroides* NapAB and the M149A variant of *Synechococcus* NarB remains to be resolved.

Met306 of *Synechococcus* NarB is absolutely conserved within the nitrate reductase and formate dehydrogenase families but has not been targeted in previous mutagenesis studies. The corresponding residue in the *D. desulfuricans* periplasmic nitrate reductase, Met308, is close (i.e., 4.4 Å) to the active-site Mo.[10] This methionine is also close (i.e., 4.7 Å) to the active-site Mo in our *in silico* model of the *Synechococcus* NarB. The observation that the M306A variant produces an essentially inactive enzyme with an approximately 40-fold decrease in the binding nitrate is consistent with the hypothesis that this residue plays an essential role in catalyzing nitrate reduction. EPR results reveal only minor perturbations of the very high-*g* proton-split Mo(V) resonance in the air-oxidized sample compared to the wild type (see Table 4 and Figures 3 and 4). However, the major changes to the high-*g* proton-split Mo(V) signal in the dithionite-reduced sample compared to that in the wild type, i.e., a change in *g* value anisotropy from rhombic to axial and complete loss of proton hyperfine coupling (see Table 4 and Figures 3 and 5), suggest that the M306 variant is no longer directly coordinated to Sγ of the active-site cysteine residue upon dithionite reduction. The latter would provide a rationale for the almost complete loss of activity (see Table 3). Most importantly, both the air-oxidized and dithionite-reduced samples are homogeneous with near complete occupancy of both cofactors and all of the Mo in each form being present as a Mo(V) species. Hence, the air-oxidized and dithionite-reduced forms of M306A *Synechococcus* NarB are attractive targets for high-resolution crystallographic studies to address the structures of the very high-*g* and high-*g* Mo(V) species, the hypothesis that loss of proton hyperfine coupling results from loss of a S_γ-coordinated cysteine residue, and the role of this rigorously conserved methionine residue in catalysis.

Arg351 in *Synechococcus* NarB corresponds to Arg354 in *D. desulfuricans* Nap, to Arg392 in *R. sphaeroides* NapAB, and to Arg421 in *Ra. eutropha* Nap. These positively charged arginine residues have been proposed to play a role in the funnel involved in guiding nitrate to the active site.[10,15,16,29,33] This is supported by the lack of activity for the R421E variant and the decreased activity (∼25% of that of the wild type) for the charge-conserving R421K variant in *Ra. eutropha* Nap.[29] In contrast, no change in activity compared to that of the wild type was observed for the R392A variant of *R. sphaeroides* NapAB, but the K_m for nitrate was increased ∼160-fold in the variant, providing strong support for a role for R392 in promoting substrate binding.[15,33] EPR studies of the R392A variant of *R. sphaeroides* NapAB revealed a 20 mV decrease in the redox potential for the $[4Fe\text{-}4S]^{2+,+}$ cluster and no Mo(V) resonances over a wide potential range.[15] The results reported herein for the R351Q and charge-conserving R351K variants of *Synechococcus* NarB concur with those for the R421E and R421K variants of *Ra. eutropha* Nap,[29] in finding greatly reduced activity compared to that of the wild type [0.3 and 6.2% for R351Q with MV and as electron donors, respectively; 1.4 and 11.5% for R351K with MV and as electron donors, respectively (see Table 3)]. However, in contrast to the dramatic increase in the K_m for nitrate observed for the R392A variant of *R. sphaeroides* NapAB, no increase in the K_d for nitrate was observed for the R351K variant of NarB, and an only modest 2.4-fold increase was observed for the R351Q variant. The observation that the R351Q variant of the *Synechococcus* NarB is almost completely inactive, but that this charge-eliminating replacement of Arg351 with Gln has an only modest effect on the affinity of the enzyme for nitrate, is consistent with the hypothesis that the side chain of Arg351 is involved in efficiently guiding nitrate toward the active site at a rate compatible with enzyme turnover, but that it is not involved in the final binding of nitrate at the active site. In addition, the observation that the charge-conserving R351K variant is effectively as inactive as the R351Q variant supports the idea that arginine is specifically required at this position and not simply a positively charged side chain. The EPR data for the NarB R351Q and R351K variants add further support to a role in guiding nitrate to the Mo center. In contrast to the lack of Mo(V) EPR signals reported for the R392A variant of *R. sphaeroides* NapAB,[15] both NarB variants investigated exhibit wild-type Mo(V) EPR signals in the air-oxidized and dithionite-reduced states, albeit with substantially diminished intensity in one form or the other (see Table 4 and Figure 3), suggesting that these mutations produce environmental perturbations that change the Mo(VI)/Mo(V) and Mo(V)/Mo(IV) redox potentials without changing the Mo coordination.

DOI: 10.1021/acs.biochem.5b00511
Biochemistry 2015, 54, 5557−5568

Asp163 in *Synechococcus* NarB corresponds Asp155 in *D. desulfuricans* Nap and Asp196 in *Ra. eutropha* Nap. Previous mutagenesis results are limited to the observation that the D196G variant of *Ra. eutropha* Nap is inactive.[29] In the *D. desulfuricans* enzyme, this aspartate forms part of the solvent-accessible funnel that leads to the Mo at the active site and may be involved in coordinating an ordered water molecule.[10] The EPR data for the D163E and D163N variants add further support for these putative roles, as both exhibit wild-type Mo(V) EPR signals in the air-oxidized and dithionite-reduced states, albeit with substantially diminished intensities (see Table 4 and Figure 3), again suggesting that these amino acid replacements produce environmental perturbations that change the Mo(VI)/Mo(V) and/or Mo(V)/Mo(IV) redox potentials without changing the Mo coordination environment. Even though the exact role of this conserved aspartate residue in nitrate reductases is still not fully understood, the data of Table 3 make it clear that there is a specific requirement for the presence of an aspartate at this position for active *Synechococcus* NarB. The observation that a charge-conserving D163E variant also lacks activity demonstrates that this requirement goes beyond a simple need for a negatively charged side chain at this position. It should be mentioned that the D163N nitrate reductase variant is the only one examined in this study that shows a significant decrease in binding affinity for both nitrate and Fd when compared to that of the wild-type enzyme. This may be related to the fact that, for reasons still not understood, there is significant loss of both Mo and Fe when Asp163 is replaced with asparagine (see Table 3). In the case of position 163, even though replacement of aspartate with glutamate does not produce an active enzyme, it does produce a variant with substrate binding affinities very similar to those of the wild-type enzyme (see Table 3).

AUTHOR INFORMATION

Corresponding Author

*Telephone: 806 834 6892. Fax: 806 742 1289. E-mail: david.knaff@ttu.edu.

Present Address

⊥S.A.: School of Medicine, Texas Tech University Health Sciences Center, Lubbock, TX 79415.

Funding

The mutagenesis, protein expression and purification, kinetic measurements, and substrate binding determinations conducted at Texas Tech University were funded by the Division of Chemical Sciences, Geosciences, and Biosciences, Office of Basic Energy Sciences of the U.S. Department of Energy, through Grant DE-FG03-99ER20346 (to D.B.K.). The *in silico* structural modeling and the Fe and Mo determinations, conducted at Arizona State University, were supported by National Science Foundation Grant CHE 11505874 (to J.P.A.). The EPR studies and analysis performed at the University of Georgia were supported by National Institutes of Health Grant GM62524 (to M.K.J.).

Notes

The authors declare no competing financial interest.

ACKNOWLEDGMENTS

We thank Mr. Wesley Caprar for conducting the Fe and Mo determinations and Prof. Enrique Flores (University of Sevilla, Sevilla, Spain) for providing the initial clone used to express the wild-type*Synechococcus* sp. PCC 7942 nitrate reductase. We also thank Prof. Luis Rubio (Polytechnical University of Madrid, Madrid, Spain) and Dr. Pierre Sétif (iBiTec-S, CNRS UMR 8221, CEA Saclay, Gif-sur-Yvette, France) for helpful discussions.

ABBREVIATIONS

CD, circular dichroism; EPR, electron paramagnetic resonance; Fd, ferredoxin; HEPES, 4-(2-hydroxyethyl)-1-piperazineethanesulfonic acid; ICP, inductively coupled plasma; IPTG, isopropyl β-D-thiogalactopyranoside; LB, Luria-Bertani; MGD, molybdopterin guanine dinucleotide; Moco, molybdenum cofactor (comprises Mo ligated by the dithiolenes of two MGD ligands in nitrate reductases); MV, methyl viologen; PCR, polymerase chain reaction; PFV, protein film voltammetry; PMSF, phenylmethanesulfonyl fluoride; SDS−PAGE, polyacrylamide gel electrophoresis in the presence of sodium dodecyl sulfate; UV, ultraviolet.

REFERENCES

(1) Hase, T., Schürmann, P., and Knaff, D. B. (2006) The interaction of ferredoxin with ferredoxin-dependent enzymes. In *Photosystem 1* (Golbeck, J. H., Ed.) pp 477−498, Springer, Dordrecht, The Netherlands.

(2) Suzuki, A., and Knaff, D. B. (2005) Nitrogen metabolism and roles of glutamate synthase in higher plants. *Photosynth. Res. 83*, 191−217.

(3) Rubio, L. M., Flores, E., and Herrero, A. (2002) Purification, cofactor analysis, and site-directed mutagenesis of *Synechococcus* ferredoxin-nitrate reductase. *Photosynth. Res. 72*, 13−26.

(4) Jepson, B. J. N., Anderson, L. J., Rubio, L. M., Taylor, C. J., Butler, C. S., Flores, E., Herrero, A., Burt, J. N., and Richardson, D. J. (2004) Tuning a nitrate reductase for function. The first spectropotentiometric characterization of a bacterial assimilatory nitrate reductase reveals novel redox properties. *J. Biol. Chem. 279*, 32212−32218.

(5) Srivastava, A. P., Hirasawa, M., Bhalla, M., Chung, J.-S., Allen, J. P., Johnson, M. K., Tripathy, J. N., Rubio, L. M., Vaccaro, B., Subramanian, S., Flores, E., Zabet-Moghaddam, M., Stitle, K., and Knaff, D. B. (2013) The roles of four conserved basic amino acids in a ferredoxin-dependent cyanobacterial nitrate reductase. *Biochemistry 52*, 4343−4353.

(6) Hirasawa, M., Rubio, L. M., Griffin, J. L., Flores, E., Herrero, A., Li, J., Kim, S.-K., Hurley, J. K., Tollin, G., and Knaff, D. B. (2004) Complex formation between ferredoxin and *Synechococcus* ferredoxin:nitrate oxidoreductase. *Biochim. Biophys. Acta, Bioenerg. 1608*, 155−162.

(7) Kisker, C., Schindelin, H., and Rees, D. C. (1997) Molybdenum-cofactor containing enzymes: Structure and mechanism. *Annu. Rev. Biochem. 66*, 233−267.

(8) João Romão, M., Moura, J. J. G., Knäblein, J., and Huber, R. (1997) Structure and function of molybdopterin containing enzymes. *Prog. Biophys. Mol. Biol. 68*, 121−144.

(9) Boyington, J. C., Gladyshev, V. N., Khangulov, S. V., Stadtman, T. C., and Sun, P. D. (1997) Crystal structure of formate dehydrogenase H: Catalysis involving Mo, molybdopterin, selenocysteine, and an Fe_4S_4 cluster. *Science 275*, 1305−1308.

(10) Dias, J. M., Than, M. E., Humm, A., Huber, R., Bourenkov, G. P., Bartunik, H. D., Bursakov, S., Calvete, J., Caldeira, J., Carneiro, C., Moura, J. J. G., Moura, I., and Romão, M. J. (1999) Crystal structure of the first dissimilatory nitrate reductase at 1.9 Å solved by MAD methods. *Structure 7*, 65−79.

(11) Raaijmakers, H., Macieira, S., Dias, J. M., Teixeira, S., Bursakov, S., Huber, R., Moura, J. J. G., Moura, I., and Ramão, M. J. (2002) Gene sequence and the 1.8Å crystal structure of the tungsten-containing formate dehydrogenase from *Desulfovibrio gigas*. *Structure 10*, 1261−1272.

DOI: 10.1021/acs.biochem.5b00511
Biochemistry 2015, 54, 5557−5568

(12) Arnoux, P., Sabaty, M., Alric, J., Frangioni, B., Guigliarelli, B., Adriano, J.-M., and Pignol, D. (2003) Structural and redox plasticity in the heterodimeric periplasmic nitrate reductase. *Nat. Struct. Biol. 10*, 928−934.
(13) Raaijmakers, H. C. A., and Romão, M. J. (2006) Formate-reduced *E. coli* formate dehydrogenase H: the reinterpretation of the crystal structure suggests a new reaction mechanism. *JBIC, J. Biol. Inorg. Chem. 11*, 849−854.
(14) Jepson, B. J. N., Mohan, S., Clarke, T. A., Gates, A. J., Cole, J. A., Butler, C. S., Butt, J. N., Hemmings, A. M., and Richardson, D. J. (2006) Spectropotentiometric and structural analysis of the periplasmic nitrate reductase from *Escherichia coli*. *J. Biol. Chem. 282*, 6425−6427.
(15) Dementin, S., Arnoux, P., Frangioni, B., Grosse, S., Leger, C., Burlat, B., Guigliarelli, B., Sabaty, M., and Pignol, D. (2007) Access to the active site of periplasmic nitrate reductase: Insights from site-directed mutagenesis and zinc inhibition studies. *Biochemistry 46*, 9713−9721.
(16) Najmudin, S., González, P. J., Trincão, J., Coelho, C., Mukhopadhyay, A., Cerqueira, N. M., Romão, F. S. A., Moura, I., Moura, J. J. G., Brondino, C. D., and Romão, M. J. (2008) Periplasmic nitrate reductase revisited: a sulfur atom completes the sixth coordination of the catalytic molybdenum. *JBIC, J. Biol. Inorg. Chem. 13*, 737−753.
(17) Coelho, C., González, P. J., Moura, J. J. G., Moura, I., Trincão, J., and João Romão, M. (2011) The crystal structure of *Cupriavidus necator* nitrate reductase in oxidized and partially reduced states. *J. Mol. Biol. 408*, 932−948.
(18) Tagawa, K., and Arnon, D. I. (1962) Ferredoxins as electron carriers in photosynthesis and in the biochemical production and consumption of hydrogen gas. *Nature 195*, 537−543.
(19) Bradford, M. M. (1976) A rapid and sensitive for the quantitation of microgram quantities of protein utilizing the principle of protein-dye binding. *Anal. Biochem. 72*, 248−254.
(20) Aasa, R., and Vänngård, T. (1975) EPR signal intensity and powder shapes: A reexamination. *J. Magn. Reson. 19*, 308−315.
(21) Fourmond, V., Burlat, B., Dementin, S., Arnoux, P., Sabaty, M., Boiry, S., Guigliarelli, B., Bertrand, P., Pignol, D., and Léger, C. (2008) Major Mo(V) EPR signature of *Rhodobacter sphaeroides* periplasmic nitrate reductase arising from a dead-end species that activates upon reduction. Relation to other molybdoenzymes from the DMSO reductase family. *J. Phys. Chem. B 112*, 15478−15486.
(22) Johnson, M. K., Duderstadt, R. E., and Duin, E. C. (1999) Biological and synthetic $[Fe_3S_4]$ clusters. *Adv. Inorg. Chem. 47*, 1−82.
(23) González, P. J., Rivas, M. G., Brondino, C. D., Bursakov, S. A., Moura, I., and Moura, J. J. G. (2006) EPR and redox properties of periplasmic nitrate reductase from *Desulfovibrio desulfuricans* ATCC 27774. *JBIC, J. Biol. Inorg. Chem. 11*, 609−616.
(24) Field, S., Thornton, N. P., Anderson, L. J., Gates, A. J., Reilly, A., Jepson, B. J. N., Richardson, D. J., George, S. J., Cheesman, M. R., and Butt, J. N. (2005) Reductive activation of nitrate reductases. *Dalton Trans.*, 3580−3586.
(25) Jacques, J. G. J., Fourmond, V., Arnoux, P., Sabaty, M., Etienne, E., Grosse, S., Biaso, F., Bertrand, P., Pignol, D., Léger, C., Guigliarelli, B., and Burlat, B. (2014) Reductive activation in periplasmic nitrate reductase involves chemical modifications of the Mo-cofactor beyond the first coordination sphere of the metal ion. *Biochim. Biophys. Acta, Bioenerg. 1837*, 277−286.
(26) Biaso, F., Burlat, B., and Guigliarelli, B. (2012) DFT investigation of the molybdenum cofactor in periplasmic nitrate reductases: Structure of the Mo(V) EPR-active species. *Inorg. Chem. 51*, 3409−3419.
(27) Butler, C. S., Fairhurst, S. A., Ferguson, S. J., Thomson, A. J., Berks, B. S., Richardson, D. J., and Lowe, D. J. (2002) Mo(V) co-ordination in the periplasmic nitrate reductase from Paracoccus pantotrophus probed by electron nuclear double resonance (ENDOR) spectroscopy. *Biochem. J. 363*, 817−823.
(28) Cerqueira, N. M. F. S. A., Gonzalez, P. J., Brondino, C. D., Romão, M. J., Romão, C. C., Moura, I., and Moura, J. J. G. (2009) The effect of the sixth sulfur ligand in the catalytic mechanism of periplasmic nitrate reductase. *J. Comput. Chem. 30*, 2466−2484.
(29) Hettmann, T., Siddiqui, R. A., Frey, C., Santos-Silva, T., Romão, M. J., and Diekmann, S. (2004) Mutagenesis study on amino acids around the molybdenum centre of the periplasmic nitrate reductase from *Ralstonia eutropha*. *Biochem. Biophys. Res. Commun. 320*, 1211−1219.
(30) Ellis, P. J., Conrads, T., Hille, R., and Kuhn, P. (2001) Crystal structure of the 100-kDa arsenite oxidase from *Alcaligenes faecalis* in two crystal forms at 1.64 Å and 2.03 Å. *Structure 9*, 125−132.
(31) Conrads, T., Hemann, C., George, G. N., Pickering, I. J., Prince, R. C., and Hille, R. (2002) The active site of arsenite oxidase from *Alcaligenes faecalis*. *J. Am. Chem. Soc. 124*, 11276−11277.
(32) Hoke, K. R., Cobb, N., Armstrong, F. A., and Hille, R. (2004) Electrochemical studies of arsenite reductase: An unusual example of a highly cooperative two-electron molybdenum center. *Biochemistry 43*, 1667−1674.
(33) Fourmond, V., Burlat, B., Dementin, S., Sabaty, M., Arnoux, P., Étienne, E., Guigliarelli, B., Bertrand, P., Pignol, D., and Léger, C. (2010) Dependence of catalytic activity on driving force in solution assays and protein film voltammetry: Insights from the comparison of nitrate reductase mutants. *Biochemistry 49*, 2424−2432.

DOI: 10.1021/acs.biochem.5b00511
Biochemistry 2015, 54, 5557−5568